Reversal modes in magnetic nanotubes

P. Landeros, S. Allende, J. Escrig, E. Salcedo, and D. Altbir[a)]
Departamento de Física, Universidad de Santiago de Chile (USACH), Av. Ecuador 3493, Santiago, Chile 917–0124

E. E. Vogel
Departamento de Ciencias Físicas, Universidad de la Frontera, Casilla 54-D, Temuco, Chile 481–1230

(Received 8 November 2006; accepted 3 January 2007; published online 5 March 2007)

The magnetic switching of ferromagnetic nanotubes is investigated as a function of their geometry. Two independent methods are used: Numerical simulations and analytical calculations. It is found that for long tubes the reversal of magnetization is achieved by two mechanisms: The propagation of a transverse domain wall or propagation of a vortex domain wall depending on the internal and external radii of the tube. © *2007 American Institute of Physics*. [DOI: 10.1063/1.2437655]

During the last decade, interesting properties of magnetic nanowires have attracted great attention. Besides their basic properties, there is evidence that they can be used in the production of magnetic devices. More recently, magnetic nanotubes have been grown[1–4] motivating intense research in the field. Magnetic measurements,[3] numerical simulations,[4] and analytical calculations[5] on such tubes have identified two main states: an in-plane magnetic ordering, namely, the flux-closure vortex state, and a uniform state with all the magnetic moments pointing parallel to the axis of the tube. It is important to establish the way and conditions for reversing the orientation of the magnetization. Although the reversal process is well known for ferromagnetic nanowires,[6–10] the equivalent phenomenon in nanotubes has been poorly explored in spite of some potential advantages over solid cylinders. Nanotubes exhibit a core-free magnetic configuration leading to uniform switching fields, guaranteeing reproducibility,[4,5] and due to their low density they can float in solutions making them suitable for applications in biotechnology.[1]

Let us consider a ferromagnetic nanotube in a state with the magnetization $\mathbf{M}$ along the tube axis. A constant and uniform magnetic field is then imposed antiparallel to $\mathbf{M}$. After some delay time the magnetization reversal (MR) will start at any end. MR can occur by means of different mechanisms, depending on the geometrical parameters of the tube. In this letter we will focus on the reversal process by means of two different but complementary approaches: numerical simulations and analytical calculations. Their mutual agreement sustains the results reported in this study.

Geometrically, tubes are characterized by their external and internal radii, R and a, respectively, and height H. It is convenient to define the ratio $\beta \equiv a/R$, so that $\beta=0$ represents a solid cylinder and $\beta \to 1$ corresponds to a very narrow tube. The internal energy E of a nanotube with N magnetic moments can be written as $E=\sum_{i=1}^{N}\sum_{j>i}^{N}(E_{ij}-J_{ij}\hat{\boldsymbol{\mu}}_i\cdot\hat{\boldsymbol{\mu}}_j)+E_a$, where E_{ij} is the dipolar energy given by $E_{ij}=[\boldsymbol{\mu}_i\cdot\boldsymbol{\mu}_j-3(\boldsymbol{\mu}_i\cdot\hat{\mathbf{n}}_{ij})(\boldsymbol{\mu}_j\cdot\hat{\mathbf{n}}_{ij})]/r_{ij}^3$, with r_{ij} the distance between the magnetic moments $\boldsymbol{\mu}_i$ and $\boldsymbol{\mu}_j$, $\hat{\boldsymbol{\mu}}_i$ the unit vector along the direction of $\boldsymbol{\mu}_i$, and $\hat{\mathbf{n}}_{ij}$ the unit vector along the direction that connects $\boldsymbol{\mu}_i$ and $\boldsymbol{\mu}_j$. $J_{ij}=J$ is the exchange coupling constant between nearest neighbors. $E_a=-\sum_{i=1}^{N}\boldsymbol{\mu}_i\cdot\boldsymbol{H}_a$ is the contribution of the external magnetic field. In this letter we are interested in soft magnetic materials, in which case anisotropy can be safely neglected.[1,4] We consider nickel tubes with $|\boldsymbol{\mu}_i|=0.61\mu_B$, lattice parameter $a_0=3.52$ Å, and $J=3.5$ meV. Dimensions are $R=15$ nm and $H=0.5$ μm, assuming a growth along the [100] direction of a fcc lattice. Tubes in the above mentioned range of sizes have at least 10^8 atoms. In order to reduce the number of interacting atoms, we make use of the scaling technique presented before,[11] applied to the calculation of the phase diagram of cylindrical particles. The authors showed that such diagram is equivalent to the one of a smaller particle with linear dimensions $d'=d\chi^{\eta}$, with $\chi<1$ and $\eta\approx 0.55$, if the exchange constant has been also scaled as $J'=\chi J$. It has also been shown[12] that the scaling relations can be used together with Monte Carlo (MC) simulations to obtain a general magnetic state of a nanoparticle. We use this idea starting from the desired value for the total number of interacting particles we can deal with, which based on the computational facilities currently available, is around 3000. With this in mind we have obtained $\chi \sim 10^{-3}$, that leads to tubes with around 10^3 atoms.

We will simulate the reversal process at temperature $T=300$ K using the scaling technique described above. MC simulations were carried out using the Metropolis algorithm with local dynamics and single-spin flip methods.[13] The effect of scaling on temperature at which the simulation are carried out have been explained by Bahiana *et al.*[14] We perform simulations for tubes characterized by β ranging from 0.17 to 0.83, starting with the saturated magnetization along the cylindrical axis, the $\hat{\mathbf{z}}$ axis, with the external field $\boldsymbol{H}_a$ applied in the $-\hat{\mathbf{z}}$ direction. Since the nucleation of a domain wall is more likely to occur at the ends, and we wish to follow the propagation of a single wall,[6] the field has not been applied to the last 12 nm of one end, following a pinning procedure used in experiments with microwires. For every β we tried $|\boldsymbol{H}_a|=1.3$, 1.5, and 1.7 kOe, without any significant difference in the results. At least five seeds were used for each set of $\boldsymbol{H}_a$ and β.

The results of our simulations and previous results in wires[7–10] show three main idealized types of MR, where $\mathbf{M}$ changes from one of its two energy minima ($\mathbf{M}=M_0\hat{\mathbf{z}}$) to the other ($\mathbf{M}=-M_0\hat{\mathbf{z}}$) by a path such that the energy barrier is the difference between the energy maximum ($E_{\max}$) and the energy minimum (E^F). These mechanisms are illustrated in Fig.

[a)]Electronic mail: daltbir@lauca.usach.cl

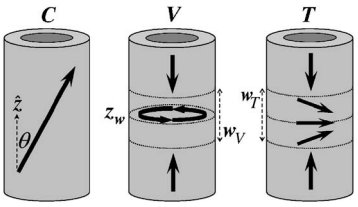

FIG. 1. Magnetic switching modes in nanotubes.

1 and correspond to *coherent rotation*, *C*, where all the spins (local magnetic moments) rotate simultaneously; *vortex wall*, *V*, where spins rotate progressively via propagation of a vortex domain wall; and *transverse wall*, *T*, where spins rotate progressively via propagation of a transverse domain wall.

We adopt a simplified description of the system in which the discrete distribution of magnetic moments is replaced by a continuous one, defined by a function $\mathbf{M}(\mathbf{r})$ such that $\mathbf{M}(\mathbf{r})\delta v$ gives the total magnetic moment within the element of volume δv centered at $\mathbf{r}$. The total energy for each mode is given by the sum of exchange and dipolar contributions, which now are taken from the continuum theory of ferromagnetism.[15] The exchange term is given by $E_{\mathrm{ex}} = A\int\Sigma(\nabla m_i)^2 dv$, with $m_i = M_i/M_0$ $(i=x,y,z)$ the components of the magnetization normalized to the saturation value M_0 and A the stiffness constant. The dipolar contribution is $E_d = (\mu_0/2)\int \mathbf{M}\cdot\nabla U dv$, with U the magnetostatic potential.[15] We will proceed to describe the magnetization $\mathbf{m}^k$ and evaluate the total energy E^k for $k=C,T$, or V.

For a uniformly magnetized tube with $m_z^C = \cos\theta$, the exchange energy is zero, and the total energy corresponds to the dipolar one given by $E^C(\theta) = \pi\mu_0 M_0^2 HR^2(1-\beta^2)[\sin^2\theta + (3\cos^2\theta - 1)N_z]/4$, where N_z is given by[5]

$$N_z = \frac{2/H}{1-\beta^2}\int_0^\infty \frac{1-e^{-qH}}{q^2}[J_1(qR) - \beta J_1(\beta qR)]^2 dq.$$

J_p represents a Bessel function of the first kind and order p. Thus for long tubes,[5] $E^C(\theta)$ has minima at $\theta=0$ and $\theta=\pi$. That is, $E^C(0) = E^C(\pi) \equiv E^F$ corresponds to the energy of a single domain ferromagnetic configuration along the axis.

In the *V* mode the magnetization can be written as

$$\mathbf{m}^V(z) = \begin{cases} \hat{\mathbf{z}}, & 0 \leqslant z \leqslant z_w - w/2 \\ m_\phi(z)\hat{\boldsymbol{\phi}} + m_z(z)\hat{\mathbf{z}}, & z_w - w/2 \leqslant z \leqslant z_w + w/2 \\ -\hat{\mathbf{z}}, & z_w + w/2 \leqslant z \leqslant H. \end{cases}$$

In this expression $z=z_w$ denotes the position of the center of the domain wall—of size w—that is, the height at which the magnetization lies totally in the xy plane describing a perfect vortex. We model the magnetization inside the wall with the functional $m_z(z) = \cos\Theta(z)$, with $\Theta(z) = \pi((z-z_w)/w + 1/2)$, which describes correctly the instantaneous shape of the vortex wall in our numerical simulations. Using $m_x = -m_\phi(z)\sin\phi$ and $m_y = m_\phi(z)\cos\phi$, the exchange energy results in $E_{\mathrm{ex}}^V = \pi A w \ln(1/\beta) + \pi^3 AR^2(1-\beta^2)/w$. The dipolar contribution can be written as

$$E_d^V = \pi\mu_0 M_0^2 R^2 \int_0^\infty \frac{dq}{q^2}[J_1(qR) - \beta J_1(\beta qR)]^2 (f_s + f_v),$$

where, $f_s = f_s(w,z_w)$ and $f_v = f_v(w,z_w)$ are related to the surface and volumetric dipolar energies, respectively, and are given by

$$f_s \equiv 1 + e^{-qH} - \frac{e^{-q(H-z_w)} + e^{-qz_w}}{1 + q^2w^2/\pi^2}\cosh\left[\frac{qw}{2}\right],$$

$$f_v \equiv \frac{qw/2 - (e^{-q(H-z_w)} + e^{-qz_w})\cosh[qw/2]}{1 + q^2w^2/\pi^2} + \frac{1 + e^{-qw}}{(1 + q^2w^2/\pi^2)^2}.$$

In the *T* mode, let us orientate the $\hat{\mathbf{x}}$ axis along the transverse direction. Then, the magnetization inside the wall (see Fig. 1) can be written as $\mathbf{m}^T(z) = m_x(z)\hat{\mathbf{x}} + m_z(z)\hat{\mathbf{z}}$, $z_w - w/2 \leqslant z \leqslant z_w + w/2$, using the same geometrical notation as in the vortex wall, with w the width of the transverse wall. We model the axial component of the magnetization using $m_z(z) = \cos\Theta(z)$. The exchange energy results in $E_{\mathrm{ex}}^T = \pi^3 AR^2(1-\beta^2)/w$.The dipolar contribution gives

$$E_d^T = \pi\mu_0 M_0^2 R^2 \int_0^\infty \frac{dq}{q^2}[J_1(qR) - \beta J_1(\beta qR)]^2 (g_s + g_v),$$

with

$$g_s = \frac{q^2w^2/2\pi^2}{1 + q^2w^2/\pi^2}\left(\frac{qw}{2} + \frac{1 + e^{-qw}}{1 + q^2w^2/\pi^2}\right) + f_s$$

and $g_v(w,z_w) = f_v(w,z_w)$. The dipolar volumetric contributions of the *V* and *T* walls have the same functional form, although not necessarily the same value due to the different wall widths of each mode, both denoted by w.

With the above expressions for the energies of the different MR processes it is possible to obtain the reversal modes as a function of the geometry of the tubes. We start by calculating the energy maximum for each path, which for the *C* mode is given by $\theta = \pi/2$, whereas in the *V* and *T* modes, it occurs when the wall is in the middle of the tube, that is, for $z_w = H/2$. The energy barrier can be calculated as $\Delta E^k = E_{\max}^k - E^F$, with $E_{\max}^k$ the energy of the k mode evaluated in their respective maximum. In cases *V* and *T* we have minimized the energy with regard to the wall width w, and then we search for the reversal mode which costs less energy.

From our simulations we can conclude that, while a *T* mode is observed for $\beta \leqslant 0.33$, *V* appeared always for $\beta \geqslant 0.5$. For $\beta = 0.33$ three seeds (of a total of 15) leads to a mix behavior: The reversal process starts as *T*, turning to *V* later on. The nucleation and propagation of the wall are monitored by the value of $\bar{m}_i(z) \equiv \bar{M}_i(z)/M_0$, average value of the components of the magnetic moment at a height z relative to the saturation value. The position of the wall is determined by the maximum of $(1-|\bar{m}_z|)$ and is shown in Fig. 2. In this figure we present snapshots at two different stages of the reversal process showing the propagation of the wall along the tube for $\beta = 0.17$ (a), 0.33 (b), and 0.5 (c). The solid line represents the average axial component of the magnetization $(\bar{m}_z)$ while the other two (in-plane) components are given by the dotted and dashed lines. When m_x and m_y both average to zero we face the *V* mechanism. When one or both of these components are nonzero, it is *T* that is observed. Case (a) shows a clear *T* behavior with a helicoidal rotation of the magnetization along the tube. Case (b) shows a *T* mode at stage t_1, which is lost at t_2 where *V* is present. The last case, (c), illustrates a *V* mode along the tube.

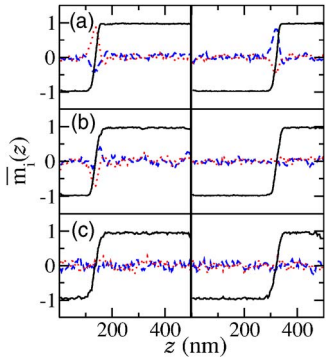

FIG. 2. (Color online) Snapshots of the reversal on tubes defined by (a) $\beta=0.17$, (b) 0.33, and (c) 0.5 at two different stages of the process. The abscissa represents the axial coordinate, z, along the tube and the ordinates give the average components of the magnetization. $\bar{m}_x$: dashed line (blue); $\bar{m}_y$: dotted line (red); $\bar{m}_z$: solid line (black).

Now we turn our attention to the results provided by our theoretical model. Upon obtaining the lowest energy barriers among the three modes we found that C is present only in very short tubes, namely, when $H \approx w$ or less. Since we are mainly interested in long tubes, as those used in experiments and applications mentioned above, we will focus our attention on T and V only. Because it is the energy of the wall which determines the reversal mode, if $H > w$ the height of the tube has no effect on the reversion process. In this case, our results show that the reversal mode depends on the internal and external radii and the magnetic material. For each β there exists a critical radius $R_c(\beta)$ at which both energy barriers, T and V, are equal. For $R < R_c(\beta)$ the tube reverses its magnetization creating a transverse wall, while for $R > R_c(\beta)$ a vortex wall appears. By equating both wall energies it is possible to obtain $R_c(\beta)$, illustrated in Fig. 3 for nickel (thick solid line), Permalloy (dashed line), cobalt, (dash-dotted line), and iron (thin solid line). Parameters for Permalloy, cobalt, and iron have been taken from Ref. 16, and those for nickel are the ones mentioned before. For $R = 15$ nm in nickel we observe that for $\beta < 0.33$ a T mode occurs, a mixed reversal behavior is observed for $\beta = 0.33$ (denoted by a dot on the Ni line), and a V mode appears for $\beta > 0.33$. These results perfectly agree with our numerical simulations (see Fig. 2).

Figure 4 illustrates our analytical results for the Ni tubes used in our simulations. Figure 4(a) depicts the energy barriers for the V and T modes as a function of β. We observed that at $\beta \approx 0.33$ the reversal mode changes from T to V, in accordance to our simulations. Figure 4(b) illustrates the corresponding wall widths for modes T and V, which are of the

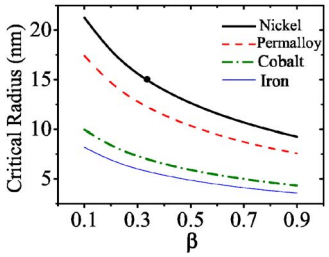

FIG. 3. (Color online) Critical radius as a function of β for different magnetic materials.

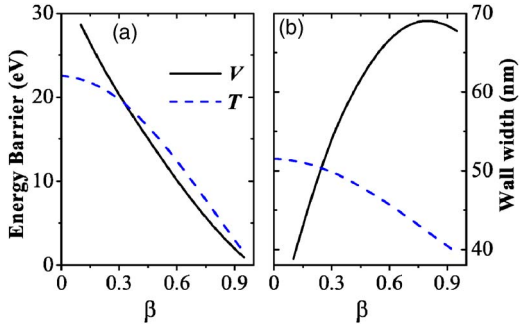

FIG. 4. (Color online) Solid lines (black) illustrate (a) the energy barriers and (b) wall width for the V mode and dashed lines (blue) correspond to the T mode.

order of nanometers. Then, for very short tubes ($H \approx w$) it is not possible to accommodate a transverse or vortex wall, giving rise to a coherent mode of reversal.

In conclusion, there are two basic reversion processes in long ferromagnetic nanotubes depending on the radii of the tube. The transverse mechanism is present in tubes with $R < R_c(\beta)$ while for tubes with $R > R_c(\beta)$ it is always the vortex mode that controls the magnetization reversal. For values of R and β close to the boundary between the two phases, instabilities arise and changes between T and V modes can occur during the process of reversion. Because nanotubes with radius smaller than 20 nm are difficult to fabricate at present,[1–3] we can conclude that the vortex reversal mode is the most observed.

This work has been partially supported by FONDECYT under Grant Nos. 1050013 and 1060317 and Millennium Science Nucleus "Condensed Matter Physics" P02-054F of Chile. CONICYT Ph.D. Program Fellowships and MECESUP USA0108 project are also acknowledged.

[1] K. Nielsch, F. J. Castaño, C. A. Ross, and R. Krishnan, J. Appl. Phys. **98**, 034318 (2005).
[2] Kornelius Nielsch, Fernando J. Castaño, Sven Matthias, Woo Lee, and Caroline A. Ross, Adv. Eng. Mater. **7**, 217 (2005).
[3] M. Daub, M. Knez, U. Gösele, and K. Nielsch, J. Appl. Phys. (accepted).
[4] Z. K. Wang, H. S. Lim, H. Y. Liu, S. C. Ng, M. H. Kuok, L. L. Tay, D. J. Lockwood, M. G. Cottam, K. L. Hobbs, P. R. Larson, J. C. Keay, G. D. Lian, and M. B. Johnson, Phys. Rev. Lett. **94**, 137208 (2005).
[5] J. Escrig, P. Landeros, D. Altbir, E. E. Vogel, and P. Vargas, J. Magn. Magn. Mater. **308**, 233 (2007).
[6] R. Varga, K. L. Garcia, M. Vázquez, and P. Vojtanik, Phys. Rev. Lett. **94**, 017201 (2005).
[7] D. Hinzke and U. Nowak, J. Magn. Magn. Mater. **221**, 365 (2000).
[8] H. Forster, T. Schrefl, D. Suess, W. Scholz, V. Tsiantos, R. Dittrich, and J. Fidler, J. Appl. Phys. **91**, 6914 (2002).
[9] R. Wieser, U. Nowak, and K. D. Usadel, Phys. Rev. B **69**, 064401 (2004).
[10] K. Nielsch, R. Hertel, R. B. Wehrspohn, J. Barthel, J. Kirschner, U. Gösele, S. F. Fischer and H. Kronmüller, IEEE Trans. Magn. **38**, 2571 (2002).
[11] J. d'Albuquerque e Castro, D. Altbir, J. C. Retamal, and P. Vargas, Phys. Rev. Lett. **88**, 237202 (2002).
[12] P. Vargas, D. Altbir, and J. d'Albuquerque e Castro, Phys. Rev. B **73**, 092417 (2006).
[13] K. Binder and D. Heermann, *Monte Carlo Simulation in Statistical Physics* (Springer, Berlin, 2002), Chap. 2, p. 5.
[14] M. Bahiana, F. S. Amaral, S. Allende, and D. Altbir, Phys. Rev. B **74**, 174412 (2006).
[15] A. Aharoni, *Introduction to the Theory of Ferromagnetism* (Clarendon, Oxford, 1996), Chap. 6, p. 111 and Chap. 7, p. 135.
[16] R. C. O'Handley, *Modern Magnetic Materials* (Wiley, New York, 2000), 99 and p. 122.